Equilibrium vacancy concentrations in Al-$\Sigma=33(554)[1\bar{1}0]$ by grand canonical Monte Carlo simulations

Emmanouil Vamvakopoulos*
Centre Européen de Calcul Atomique et Moléculaire, Ecole Normale Supérieure de Lyon, 46 allée d'Italie, 69007 Lyon, France

Döme Tanguy†
CNRS, UMR 5146, Ecole des Mines de Saint-Etienne, 158 cours Fauriel, 42 023 Saint-Etienne, France
(Received 1 December 2008; published 26 March 2009)

A Monte Carlo simulation of equilibrium thermal vacancies is extended to grain boundaries in Al. The vacancy localization is explored by intensive molecular-dynamics simulations. It is found that, in the symmetrical tilt boundary $\Sigma=33(554)[1\bar{1}0]$, the reference lattice, based on the coincident site lattice geometrical model, is good enough to describe the microstates of the system up to $T=700$ K in the presence of vacancies and vacancy clusters. A microstate is therefore defined by site occupancies and continuous displacements from the lattice nodes. This model, intermediate between an Ising model and the representation of states in classical statistical mechanics, is used to perform grand canonical Monte Carlo simulations. Vacancy concentrations along the grain boundary are computed from the average site occupancies. Vacancy alignment along the tilt axis is reported. The results are analyzed in the framework of a one-dimensional Ising model which incorporates vacancy free formation energies and pair interaction free energies.

DOI: 10.1103/PhysRevB.79.094116 PACS number(s): 61.72.Bb, 02.70.Uu, 61.72.J−

I. INTRODUCTION

Vacancies play an important role in crystalline solids, in particular in metals and alloys where they influence optical, electrical, and mechanical properties.[1] These defects are the vector of solid-state diffusion which leads to the formation of the microstructure by phase precipitation. Microstructure, in turn, largely controls mechanical properties via dislocation-precipitate interactions in precipitate hardened alloys. But vacancies can also affect directly the alloy's mechanical response through their interaction with extended defects such as dislocations, in fatigue, for example, and grain boundaries (GBs),[2] especially when the GBs are coupled to solute interstitials.[3,4] The tendency of vacancies to act as a trap for solute interstitials can lead to spectacular vacancy concentrations, in particular in H containing systems where these vacancies are in fact vacancy-hydrogen complexes called superabundant vacancies.[5,6]

A method predicting equilibrium vacancy concentration in complex crystalline structures such as semicoherent interfaces or GB submitted to solute segregation would be a valuable asset to model intergranular precipitation and GB loss of strength. The thermodynamic quantities which describe vacancies in equilibrium can be extracted from free-energy calculations. Several methods have been proposed to determine free-energy differences. Approximate calculations of vacancy formation free energy in the framework of lattice dynamics theory provide a reasonable compromise between accuracy and computational demand.[7] These methods can be used to describe vacancies in systems where the anharmonicity effects is not too large.[8] In addition, thermodynamic integration schemes based on Monte Carlo (MC) or molecular-dynamics (MD) methods where the anharmonicity effects are described directly can be used. These schemes require good statistical accuracy in the computed averages of the enthalpy of the system with and without the defects.[9,10] Furthermore, the transferability of the semiempirical potentials is always a delicate issue, especially when it comes to describing the enhanced anharmonicity through the presence of defects.[11,12]

In a previous work,[13] we developed a grand canonical (GC) Monte Carlo method to compute superabundant vacancy concentrations in bulk fcc. The method consists of a three-dimensional (3D) Ising type model with a fixed number of lattice sites coupled with continuous degree of freedom. In the pure metal, this method gives access to the vacancy formation free energies if they are extracted from the concentrations with the use of a lattice-gas model.[14] Even if the method is computationally heavy for the moment since it relies on insertions/deletions of particles in dense systems, it aims at performing grand canonical simulation on any kind of crystalline defects, extending the range of segregation studies to complex interfaces. In this paper, we present the extension of this method and the calculation of equilibrium vacancy concentrations in a grain boundary. In the following section, a short description of the method and of the motivation of the theory is given. Then, the computational methodology and the structure of the GB are presented. Next, results concerning the localization of the vacancies on the GB sites, obtained by molecular-dynamics simulation, are shown. Finally, equilibrium vacancy concentrations are produced by grand canonical Monte Carlo simulations. These are analyzed by combined free-energy calculations and the analytical solution for the cluster distribution of a one-dimensional (1D) Ising model. Free binding energies for vacancies are reported which illustrate the formation of vacancy lines along the tilt axis.

II. METHODS

We want to go beyond the calculation of the properties of an isolated vacancy, and construct a brute force numerical

method to treat the equilibrium of clusters of vacancies and their interaction with other crystalline defects (dislocations, grain boundaries, and solute interstitials). More specifically, we want a method capable of describing reconstructions. Surface reconstruction can, to some extent, be treated by canonical Monte Carlo where atoms from the surface plane can be explicitly moved to adatom positions or an adsorbed line of atoms (see Ref. 15 and references therein). In order to treat interface reconstruction, the calculation should be brought to the grand canonical description because Frenkel pairs are energetically expensive in metallic systems and therefore rare. Certainly the most general approach is the one proposed by Swope and Andersen[16] where a bias is introduced in the way the particles are chosen for deletion and the cavities are detected for insertion. This bias relies on a decomposition of the volume of the system on a refined grid which plays no role in the definition of the microstate of the system and can be of arbitrary shape not related to the stable structure of the crystal. It has been used with success to determine the metastable states in a transition from a dense liquid to a solid in two-dimensional,[17] a pathological case where it is extremely difficult for a numerical method to produce enough statistics. In the more specific case of the GB, the issue is subtle because a GB is a metastable state of the crystal where the geometrical parameters (misorientation and interface plane) are fixed and can be considered as constraints. The other degrees of freedom, such as the position of the particles and the relative translations of one crystal with respect to the other, are free in (N,V,T) or (N,P,T) ensembles. Under these constraints, the GB structure is composed of stable structural units (SUs) but they are not free from allotropic transformations[18] and a GB can be composed of a mixture of SU of vicinal excess free energy.[19] In this context, defining a vacancy implicitly means that the SU is stable at the temperature considered and that removing a few particles will not lead to drastic structure changes. Otherwise the reference structure is not stable and there is no meaning to give to the notion of vacancy.

In this work, we perform GC Monte Carlo; hence we release the number of particles at fixed volume and fixed geometrical parameters of the GB, including relative translations. The grid used is the Voronoi decomposition of space based on the coincidence site lattice model, in other words, on the stable structure obtained in (N,V,T) ensemble. The relevance of this decomposition is not known *a priori* and should be tested. This is done by performing MD simulations. A well-known issue is the dissolution of the vacancy. We will show that this phenomenon does not involve the breakdown of the method as long as it does not trigger a global structure change in the GB. The breakdown of the cell decomposition of space is not a conceptual issue since it is always possible to take a more refined grid, independent of the structure of the GB. But then, the meaning of the site occupancies, which relates a node position to the most probable position of the particle, is lost and the vacancy should be replaced by an excess volume.[20] The interest to stick to a reference lattice is the possibility to define lattice-gas models which can be treated analytically, and used to analyze and check the MC results, as we will do here.

A. Description of the Monte Carlo method

Following Ref. 13, a reference lattice is used which enables definition of site occupancies: $p_n=1$ if the site is occupied and zero otherwise (vacancy). If N particles are present in the system, and the lattice has M sites (or nodes) $M>N$, N occupancies are set to one while the others to zero. The N positions $\vec{r}$ of the particles are decomposed such as referencing the particle from the position of the closest node:

$$\vec{r}_n = \vec{r}_n^0 + \vec{u}_n. \tag{1}$$

$\vec{r}_n^0$ is the fixed position of the node and $\vec{u}_n$ is the displacement of the particle from that node. By construction, $\vec{u}_n$ is inside the Voronoi cell containing site n. Then a microstate, in configuration space, is defined by $(\{p_n\}^M,\{\vec{u}_n\}^N)$. Phase space is explicitly limited to the subspace where the continuous positions can be decomposed on the M lattice nodes, without multiple occupancies. In other words, the system is constrained[21] during the simulation staying in the structure defined by the lattice, with distortions which do not bring the particles out of the Voronoi cell of their node. Self interstitials are not allowed, which is not a drastic approximation because they are energetically expensive in metallic systems.[22] The constrained grand canonical partition function Q_c is, when the macrostate is defined by (M,μ,V,T):

$$Q_c(M,\mu,V,T) = \frac{1}{\Lambda^{3N}} \sum_{N=0}^{M} \sum_{P_M} \int_{V_1} d\vec{u}_1 \int_{V_2} d\vec{u}_2 \ldots \int_{V_N} d\vec{u}_N \times e^{-\beta[\mathcal{H}(\{p_n\}^M,\{\vec{u}_n\}^N)-N\mu]}, \tag{2}$$

where Λ is the thermal de Broglie wavelength, $\beta=1/kT$, and V_i is the volume of the Voronoi cell surrounding site i. The total number of particles is $N=\Sigma_{i=1}^{M} p_i$. While the use of the fcc lattice in a perfect bulk is suitable, the choice of a reference for the GB is not straightforward. The reasons why the grid can fail to define the microstates is the thermal disorder[23] which can lead to grain-boundary premelting, and the well-known issue of the vacancy dissolution which should not trigger global structure change in the GB.[24] In Sec. IV A, the temperature range where the GB structure is stable, and therefore where the grid is relevant for MC simulations, even in the presence of the most probable vacancy clusters, is tested by intensive MD simulations.

B. Monte Carlo moves

A chain of states representative of the equilibrium described by Eq. (2) is generated by a Monte Carlo procedure using the Metropolis algorithm. Trial states are proposed by performing three types of moves: particle displacements, insertion/deletion of particles in the cells (spin flips), and exchanges between a vacant and an occupied site. All these moves are designed with respect to detailed balance.[13] The particles' displacements are performed by proposing displacement increments at random with a uniform distribution, such that a random walk is performed in each occupied cell. The maximum amplitude of the displacement increment is adjusted to have 50% acceptance of the displacement moves. In the case where a new displacement brings the particle out

of its Voronoi cell, and the neighboring cell is occupied, and the trial move is early rejected. Therefore, the displacements are confined inside the Voronoi polyhedrons. The use of the grid forbids the configurations where two particles fall in the same cell. In principle, this is a limit of phase space in contrast to MD. This is why the comparison to MD is done: to check that this portions of phase space plays a negligible role.

The insertion/deletion moves of the particles are done as follows. A lattice site i is chosen at random with probability $\frac{1}{M}$ while the system is in state A. If the site i is occupied, a trial state B is proposed by setting the occupancy to zero. The reverse move implies selection of the site i, in state B, with the same probability $\frac{1}{M}$ and the insertion of a particle in the cell at the former position $\vec{u}_i$. This is done by picking a position at random, with a uniform probability, and finding $\vec{u}_i$ with a probability $d\vec{u}_i/V_i$,[16] where V_i is the volume of the cell. From the detailed balance condition,[13] the acceptance probability $\mathrm{acc}(A \rightarrow B)$ for the transition from state A (where the site i is occupied $p_i=1$) to state B (where the site i is empty $p_i=0$) at site i is given by

$$\mathrm{acc}(A \rightarrow B) = \min\left[1, \frac{V_i}{\Lambda^3} e^{-\beta[H_B - H_A - \mu]}\right], \tag{3}$$

where H_B and H_A stand for the energies of states B and A, respectively.

The exchange moves are performed in two steps between two randomly selected sites, one vacant site i and one occupied site k. First, an insertion move is performed in the cell i, with the same trial displacement as the one on site k. The energy change is ΔE_1 between the initial state A and the intermediate state C. In A, site i is empty $p_i=0$ and site k is occupied $p_k=1$. In the intermediate state C, site i and k are both occupied $p_i=p_k=1$. Second, a deletion trial move is performed at site k with an energy change ΔE_2 between state C and the final state B. In state B, site i is occupied $p_i=1$ and site k is empty $p_k=0$. The acceptance probability for the exchange move between vacant site k and occupied site i are given by the following equation:

$$\mathrm{acc}(A \rightarrow C) = e^{-\beta \Delta H}, \tag{4}$$

where $\Delta H=\Delta E_1+\Delta E_2$ is the energy change between state A ($p_i=0$ and $p_k=1$) and B ($p_i=1$ and $p_k=0$) through an intermediate state C ($p_i=1$ and $p_k=1$).

III. GRAIN-BOUNDARY STRUCTURE

The Al-$\Sigma 33(554)[1\bar{1}0]$ is chosen as a model grain boundary. The structure of this GB is studied in Ref. 19. It is composed of two different structural units D and E. The D unit is a twin and E unit is a capped trigonal prism, composed of six atoms. Because D is bulklike, it is expected that the vacancy formation energies will be more heterogeneous on the sites of the more complex E unit and that it contains the potential host sites for vacancies. An interesting feature of the family of symmetrical tilt boundaries of axis [110] is that the proportion of the E and D units can be changed by modifying the disorientation angle. In other words, the density of the potential host sites for vacancies can be tuned.

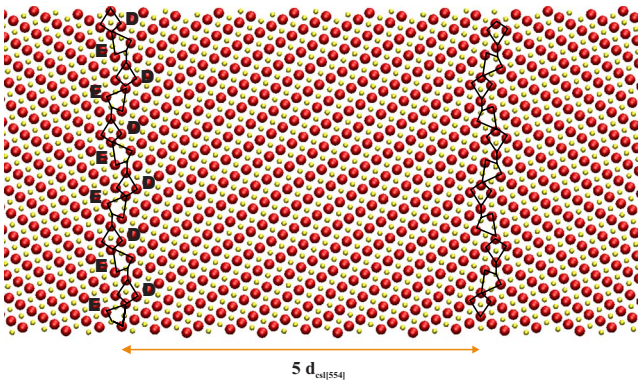

FIG. 1. (Color online) $\Sigma 33(554)[1\bar{1}0]$ grain boundary viewed along the tilt axis. The big spheres stand for the (110) planes and the small ones stand for the (220) planes. The letter stands for the structural unit in the GB core. The distance between the mathematical symmetry planes of the two GB is five times the CSL size in the [554] direction, as showed by the double arrow.

The simulations are performed with a computational cell which contains a bicrystal with the planar defect at its center. The atomic positions in the bicrystal are generated from the geometrical coincident site lattice (CSL). The use of three-dimensional periodic boundary conditions creates a second grain boundary at the edges of the computational cell normal to the [554] direction. The computational cell is composed of three CSL cells in the $[\bar{2}\bar{2}5]$ direction, ten CSL cells normal to the GB in the [554] direction, and twelve CSL cells along the tilt axis $[1\bar{1}0]$. Note that it implies that each atomic line, parallel to the tilt axis, is composed of 12 equivalent atomic sites over which averages can be taken (in particular average occupancies). In principle the averages can also be taken over the equivalent lines of the structural units. These dimensions are large enough to have a perfect bulk region in between the two GBs.

The interactions are modeled by an embedded atom potential (EAM) for Al, which was obtained by a massive fitting to a quantum database using the force matching method.[25] This model has been successfully used to study bulk, surface, and GB properties.[26–29] The lattice parameter in the directions parallel to the boundary is fixed to the bulk value at the temperature considered. The boundary energy is relaxed by adjusting the relative displacement t_x in the direction normal to the interface. Quenched molecular dynamics (QMD) is used to relax the structure at zero temperature (Fig. 1) for various values of the imposed relative displacement. The relaxed boundary energy for this structure is 289.0 $\mathrm{mJ/m^2}$ at $t_x=0.37a_0$, where $a_0=4.032$ Å is the lattice parameter of the bulk Al at 0 K. In Fig. 1, we present the relaxed GB obtained at 0 K.

The initial grid has to be defined in order to perform MC in (M, μ, V, T) constrained ensemble. The reference lattice is the relaxed structure of the GB at 0 K. At finite temperature, the positions in the direction parallel to the interface are scaled by the thermal dilation factor of the bulk. The excess GB volume is relaxed by adjusting the relative displacement t_x in the direction [554] in order to obtain zero stress in this

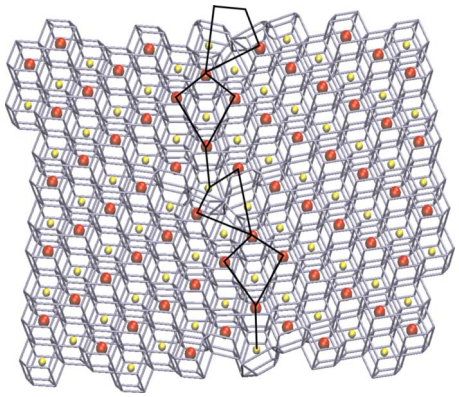

FIG. 2. (Color online) A snapshot (Ref. 30) of the grid around the $\Sigma 33(554)[1\bar{1}0]$ GB along the tilt axis. The big spheres stand for the (110) planes and the small ones stand for the (220) planes. The black traces mark the D and E units.

direction. This is obtained by translating all particles with $x_i > 0$ ($x_i < 0$) by $t_x/2$ ($-t_x/2$). $x_i = 0$ is the symmetry plane of the GB and x is the direction normal to the GB plane. The stresses are calculated by the virial theorem.

The Voronoi polyhedron decomposition of space is done by a well-established algorithm by Rapaport[31] which gives the volumes V_i used in the acceptance criterion [Eq. (3)]. A picture of the Voronoi decomposition which defines cells inside which the random walk of the particles is confined and the nodes where the occupancies are defined, is presented in Fig. 2. This grid easily defines the vacancies and will be used later to formulate a lattice-gas model[14] to check and analyze the MC results.

The vacancy formation energy E_f^v is computed, at 0 K, on every nonequivalent site of the GB. It is a way to get an idea of the heterogeneity before performing Monte Carlo simulations. In Fig. 3, the E_f^v map, at constant volume, is presented. The big and the small circles correspond, respectively, to the (110) planes and the (220) planes. The numbers correspond

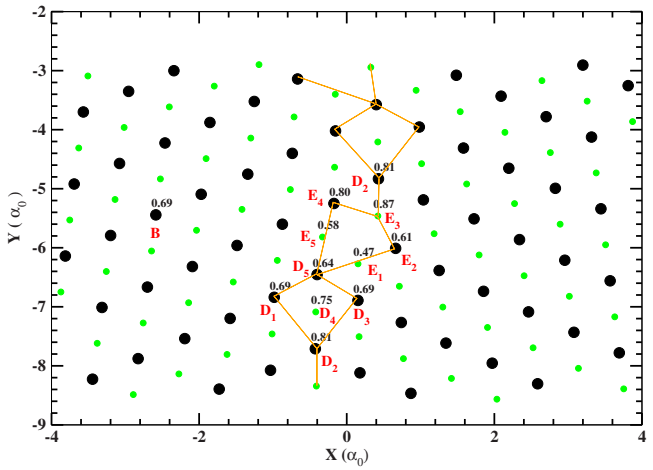

FIG. 3. (Color online) Vacancy formation energy map of the $\Sigma 33(554)[1\bar{1}0]$ GB core. The big circles stand for the (110) planes and the small ones stand for the (220) planes. The numbers stand for the vacancy formation energy in electron volts, at 0 K.

to the E_f^v on each specific site. As can be seen in Fig. 3, the sites in the E unit exhibit vacancy formation energies in the range of 0.47 eV (E_1) to 0.87 eV (E_3). On the contrary, the sites of D units present values close or greater than the bulk value (0.69 eV). The critical issue is addressed in the next section: the efficiency of the grid to define the microstates at high temperature.

IV. VACANCY CLUSTERS OBTAINED BY ALL DEGREES OF FREEDOM METHODS (MD AND MC)

A. Molecular dynamics

The thermal stability of the GB structure obtained at 0 K is checked with molecular-dynamics simulations in the microcanonical ensemble. The equations of motion are integrated by the leapfrog algorithm with a time step of 1 fs. The GB equilibration takes 60 ps which are excluded from the averages. These are performed over a simulation time of 40 ps. The temperatures investigated range from 400 K to 900 K. We can mention that the potential predicts the melting of bulk Al at 930 K, in agreement with experimental results.[25] No allotropic transition by shuffling was observed.

The degree of crystallinity of a GB structure can be quantified by following the variation with temperature of the structure factor.[23] In the case of the symmetrical $\Sigma = 5(310)[001]$ tilt boundary in Ar,[23] a smooth transition from a crystalline order similar to the one of the perfect bulk toward the one of a liquid has been observed, consistent with an increase in the self-diffusion coefficient. Nevertheless, the GB is not liquid but highly defected. The liquid state is reached only at the melting point of the bulk. In our case, the self-diffusion events are too rare, within the duration of classical MD, to allow the determination of the diffusion coefficients. Therefore, the smooth departure from a pure bulk behavior is quantified by the temperature evolution of the mean-square displacements (MSDs), along the tilt axis. The MSD is given by

$$\langle u_X^2 \rangle = \frac{1}{N_i} \sum_{i=1}^{N_i} \langle z_i^2 \rangle - \langle z_i \rangle^2, \tag{5}$$

where i stands for the site index, N_i is the number of sites in the region over which a site average is taken ($X = E$, D, or bulk), z_i is the coordinate of the particle in the direction parallel to the tilt axis, and brackets denote the time averages. In the time averages, some isolated events of self-diffusion are excluded at temperatures above 800 K. These events occur mostly on the sites of the E SU. The criterion for this exclusion is that the average displacement of the particles is greater than half the nearest-neighbor distance (the average position is outside of the Voronoi cell). During self-diffusion, no long-lived double occupancies of the Voronoi cells were observed, which would justify grid refinement for this particular GB. The system always comes back to the structure used to define the grid. We recall that we want to design an equilibrium Monte Carlo method so the microstates corresponding to rare events do not need to be captured if they don't contribute significantly to the averages of interest. For example, it is not necessary to capture saddle

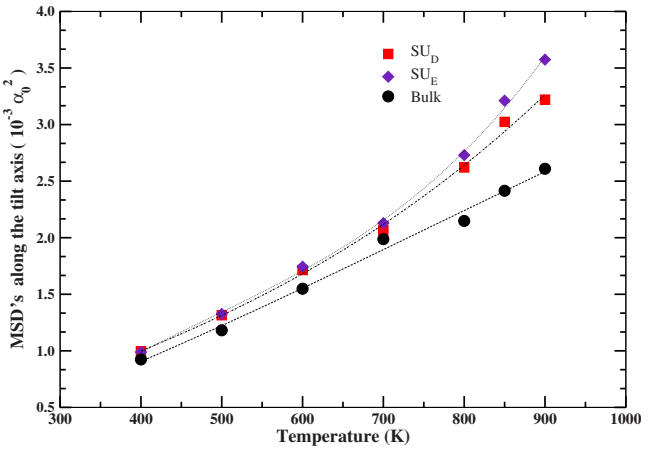

FIG. 4. (Color online) MSDs along the tilt axis, as a function of the temperature, averaged over the atoms of the D (rectangles), E units (diamonds), and bulk region (black circles). The lines are a guide to the eye. a_0 stand for the lattice constant of bulk Al at 0 K.

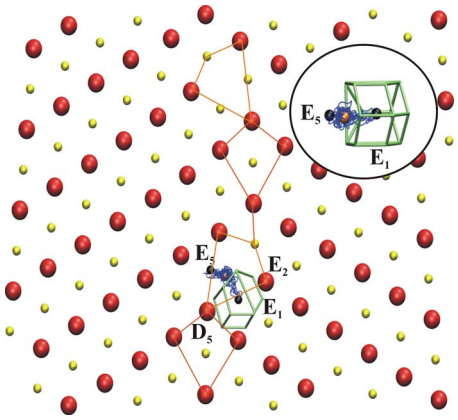

FIG. 5. (Color online) A snapshot of the GB core with a vacancy on site E_1. The letter stands for the representative sites in the GB core. The small black spheres stand for the initial position of the sites E_1 and E_5 on the initial grid. The thin line between black spheres represent a trajectory trace of the atom on site E_5.

configurations for diffusion if only the average vacancy concentrations are wanted. These are more efficiently obtained by performing spin flips and exchanges rather than following a realistic diffusion path.

Figure 4 presents the temperature dependence of the MSDs for the atoms of the D units (rectangles), the E units (diamond), and the bulk region (black circles). Along the direction of the tilt axis, the symmetry of the bulk and the grain-boundary regions is preserved and the comparison is reasonable.[23] For temperatures up to 700 K, the MSDs of the E and D SUs present a linear dependence with the temperature, similar to the bulk. Above 700 K, we can see large deviations between the GB and the bulk behavior. Further increase in the temperature, above 800 K, leads to the deviation between the E and D unit MSD values. From these results it comes out that the GB core sites of the E and D units are less tightly bonded in the direction of the tilt axis compared to the bulk atoms. The signature of this is a larger vibration amplitude. As the temperature increases above 700 K, this difference becomes more pronounced. An interesting issue is that, above 800 K, a difference between atoms of the E and D SUs also arises, which reflects a precursor of the disordering of the E SU, before the triggering of self-diffusion. At 700 K, the crystalline order still compares quite well with the perfect bulk. The MSD is of the order of $2 \times 10^{-3} a_0^2$, which, assuming a Gaussian distribution ($\sigma \approx 0.05 a_0$) of the position around the average, gives a very low probability for the particle to fall outside of the Voronoi cell [$P(r > 0.35 a_0) < 10^{-10}$]. Indeed, particles are almost never observed "bumping" on the walls of their cell. Based on this quantification of the localization of the particles and the rare event argument, $T = 700$ K is a safe temperature for MC simulations and the choice of a large grid, in comparison to the cubic square grid of Swope, is justified. $T = 700$ K is used from now on.

The efficiency of the Voronoi decomposition can be checked further by studying the relaxation of the nearest neighbors of empty sites (vacancies) in the GB core. More specifically, MD simulations are used to generate a time sequence of microstates which are then analyzed to check if they can be captured by the representation $[(\{p_n\}^M, \{\vec{u}_n\}^N)]$ used in the Monte Carlo simulations.

In the bulk, the local environment of the vacancies presents a slight relaxation which leads to the contraction of the formation volume of a vacancy. In GBs the relaxation can be so strong that it can lead to the delocalization of the vacancy.[24] This delocalization can drive the system to a global reconstruction.[32] In this part, we run a set of MD simulations in the microcanonical ensemble, each of them with a single vacancy initially on a different site of the E unit and for a duration of 200 ps at 700 K. At this temperature, according to the previous paragraph, the GB equilibrates below the onset of self-diffusion. The initial vacancy diffuses rapidly and in most simulations equilibrates on site E_1 (the site with the lowest vacancy formation energy). The vacancy lives on this site for long times, up to 100 ps. A picture of the GB core with a vacancy on site E_1 is shown on Fig. 5. The big spheres stand for the (110) planes and the small ones for the (220) planes. The letter stands for the sites index. The small black spheres represent the E_1 and E_5 nodes. The thick lines stand for the projection on (110) planes of the edges of the Voronoi polyhedron corresponding to site E_1. The two sites belong to the same (220) plane and the shared Voronoi facet is perpendicular to the plane of the figure. Node E_5, which corresponds to the mean position of the particle when E_1 is occupied, is at $0.34 a_0$ from the facet. When a vacancy is created at E_1, the atom mean position is displaced by $0.29 a_0$ toward the facet (Fig. 5), which is close the boundary between the E_1 and E_5 cells. Transitions occur periodically where the atom leaves cell E_5 and fills cell E_1. The inset on Fig. 5 presents another viewpoint of this motion. The thin line between black spheres represents the particle trajectory for a duration of 4 ps.

To have a statistical view of this motion, we calculate the probability $P(d)$ that the projection of the atom's position on the line joining the nodes E_5 and E_1 is d within some uncertainty (Fig. 6). The statistics is collected from a trajectory of length a 100 ps. The vertical lines (Fig. 6) show the positions

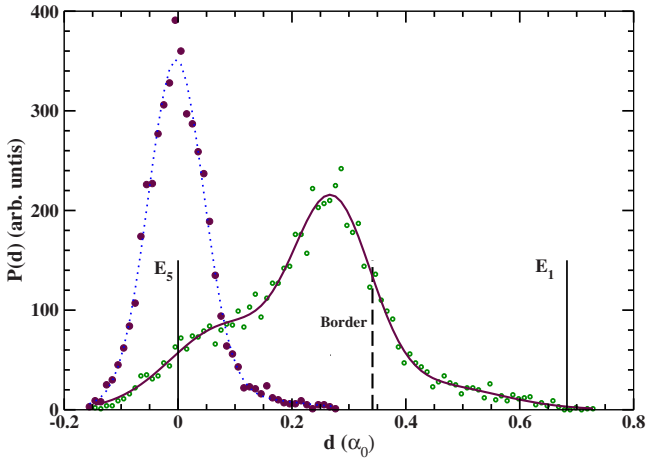

FIG. 6. (Color online) Projection of the displacement of a particle attached to node E_5, when E_1 is vacant. A short 3D trajectory is shown on Fig. 5.

of the sites E_5 and E_1. The dashed vertical line corresponds to the Voronoi border between the two sites. The filled (empty) circles represent the displacements distribution of an atom on site E_5, when E_1 is occupied (empty). When E_1 is occupied, the distribution is nicely peaked around node E_5. Whereas, when it is empty, the distribution is shifted toward E_1 and broadened. We cannot identify two peaks in the distribution that would indicate two distinct energy basins (vacancy on E_1 or E_5) from which the system could make transitions. On the contrary, there is only one state where the particle has a new equilibrium position, close to the border, but still it spends most of the time in cell E_5, and makes brief incursions in cell E_1.

In addition, MD simulations, in the microcanonical ensemble, are performed on a system containing a set of vacancies, aligned along the tilt axis. Such configuration is called a vacancy chain. Its length is varied up to six vacancies. The vacancies occupy site E_1. We calculate the volume of each vacancy from the average positions of the neighbors taken in a time window of at least 30 ps, where the vacancy chain is stable. Figure 7 shows a snapshot with a chain of length two. In this case, the relaxation of the local environment is more complex than the one of the single vacancy. Two atoms on site E_5 relax toward the vacant sites and perform again a delocalized oscillation motion. The average displacement is $0.24a_0$ for both atoms, similar to the single vacancy case. The atom on site E_2 which belongs to the (110) plane in between the vacancies (see inset of Fig. 7) relaxes close to the borders. The direction of the average displacement is normal to the tilt axis, with a norm $0.22a_0$. A similar qualitative picture is obtained for longer chains.

In Fig. 8, we present the relative volumes (with respect to the volume of the cells) of each vacant site for chains of different lengths (filled symbols). The average position of the neighbors is computed as above. The sites of the divacancy have a relative volume of 68.3%. In the trimmer, the volume of the middle site is 63% while the one of the edge sites is 69.5%. The same results hold for the longer chains: the relative volumes of the vacant edge sites are greater than those of the inner sites. In the case of the divacancy, the distribution of the relaxed neighbors is symmetric across the (110) plane (large spheres on Fig. 7). Both sites of the divacancy have one relaxed neighbor of type E_5 on the same (220) plane and one common neighbor on a site of type E_2 on the symmetry plane (inset of Fig. 7). In the case of the trimmer, the inner site has one coplanar neighbor of type E_5 and two neighbors of type E_2 from the two adjacent (110) planes. The edge sites have one neighbor of type E_5 and one of type E_2. The significant drop of the volume of the inner sites can be attributed to the number of neighbors which show strong relaxations, in preference to a difference of the amplitude of the relaxations, because these are similar.

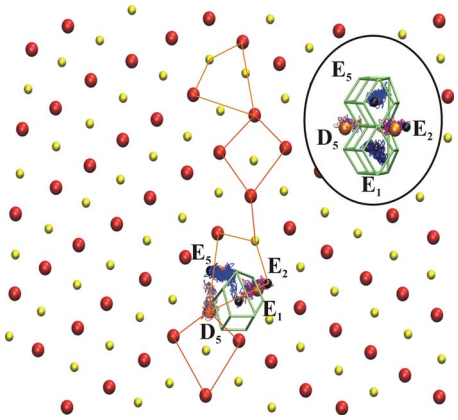

FIG. 7. (Color online) A snapshot of the GB core with two vacancies on sites of type E_1 along the tilt axis. The letters stand for the representative sites in the GB core.

The conclusion of this MD study is that the delocalized motion of the neighbors of the vacancies, or of the vacancy chains, does not lead to the formation of new lattice sites or to the annihilation of old ones. Therefore the lattice based on the equilibrium structure of the GB, without point defects, and the associated Voronoi decomposition of space, is an efficient choice to define the microstates of the system for the Monte Carlo simulations.

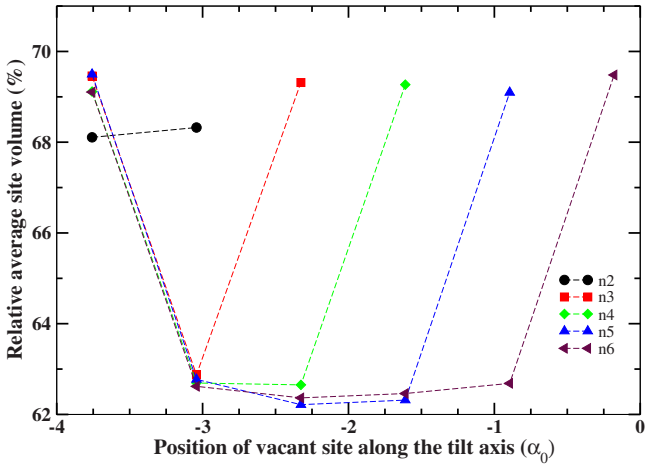

FIG. 8. (Color online) Average relative volume (with respect to initial grid) of the sites of a vacancy line with different length on site E_1, as a function of the position of the vacant site along the tilt axis

B. Monte Carlo simulations in the grand canonical constant lattice sites ensemble

We perform Monte Carlo simulations in the constant lattice site ensemble (M,μ,V,T) at $T=700$ K. The chemical potential of bulk Al was calculated by thermodynamic integration for different temperatures at the average volume which corresponds to zero pressure.[13] First, 500×10^6 MC steps, with only displacement moves, are performed to equilibrate the structure at finite temperature. Next, grand canonical MC simulations with displacement, insertion/deletion, and exchange moves are done with a number of steps up to 15×10^9. The moves involve particles a region of width $[-4,4]$ d_{544}, where d_{554} is the length of the CSL cell in the [554] direction. This region contains the core of the GB. The particles in the rest of the simulation box are kept fixed. Moreover, thirty replicas are used, with different initial seeds of the pseudorandom number generator,[33] to get better statistics. In all MC simulations, the occupancies $\{p_n\}^M$ are recorded to compute the average concentrations.

The insertion/deletion moves have a low acceptance rate of the order of 10^{-5} at $T=700$ K. In the bulk, reasonable statistics for vacancy concentration can be obtained above 600 K because all sites are equivalent. In a CSL based bicrystal, the average local concentration on each nonequivalent site of the CSL unit is averaged over all CSL units in the system to give the average site or plane concentration. With our system size, each site is represented 36 times. Equilibrium concentrations of vacancies are obtained by averaging the occupancies in three steps: an average on the equivalent sites in the system, an average over the MC steps, and an average over the replicas. In the bulk, all sites are equivalent whereas in the GB, only structural units are equivalent. The same accuracy between GB and bulk concentrations could be obtained by multiplying the reference number of the MC steps by a factor $\frac{N_{\text{bulk}}}{N_{\text{SU}}}$, where N_{bulk} is the number of particles in bulk reference simulation and N_{SU} is the number of equivalent sites of the SU over all CSL units of the system. This factor can be large. Fortunately, the acceptance ratio in the GB is not as small as in the bulk, so if $\frac{N_{\text{bulk}}}{N_{\text{SU}}}\times\frac{1}{100}\approx1$, the average concentrations per GB plane can converge.

The average vacancy concentrations per plane parallel to the interface are presented on Fig. 9 as function of the layer's position. Each GB site is represented by one point. This profile reveals the symmetrical character of the GB structure, within some minor distortions. The error bars are less than the size of the points. The higher concentrations are found on the planes close to the interface plane composed of the sites E_1, E_5, and E_2. The values are 0.31×10^{-2} and 0.30×10^{-3}, respectively. These are two orders of magnitude greater than the vacancy concentration[13] in the bulk 2.95×10^{-5}, which compares nicely with the experimental value in bulk Al at 700 K: 3.16×10^{-5}, obtained by differential dilatometry measurements.[1] The local concentrations decrease gradually to approach the bulk value as the distance from the GB symmetry plane increases. The oscillations on the profile come from an alternate participation of sites from the D and E SUs. The vacancy free formation energy can be calculated on each site by inverting the formula obtained by a lattice-gas model for isolated vacancies:[14]

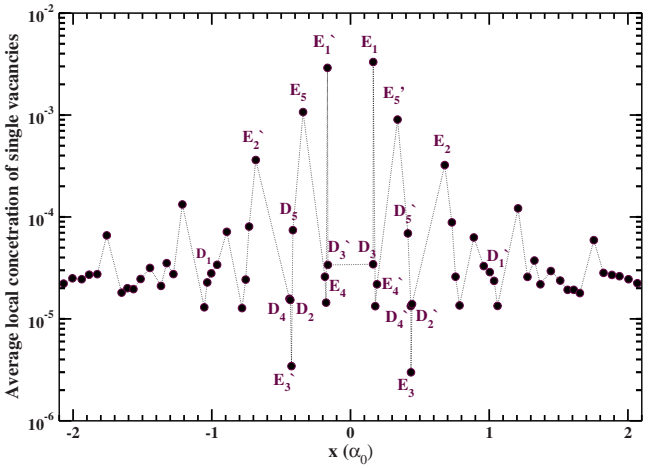

FIG. 9. (Color online) Single vacancy concentration profile in the direction [554] normal to the interface at $T=700$ K. The dotted line is to guide the eyes.

$$c_i = e^{-g_v^i/k_BT}, \tag{6}$$

where c_i is the local average concentration of single vacancies obtained by MC and g_v^i is the free vacancy formation energy at site i. A map of these energies is shown on Fig. 10 where the sites of the D and E SUs are represented.

As we can see in Fig. 10, the sites in the SU E labeled E_1, E_2, and E_5 have g_v^i values lower than the bulk (0.63 eV). At site E_1, g_v^i is minimal 0.35 eV, whereas at sites E_2 and E_5, g_v^i are a little higher: 0.48 and 0.41 eV, respectively. Moreover, the sites which form the D units have greater or equivalent g_v^i values than the bulk. At site D_2, g_v^i is 0.67 eV while at the sites D_4 and D_3 the values are 0.67 and 0.62 eV, respectively. Compared to the vacancy formation energy at zero kelvins,

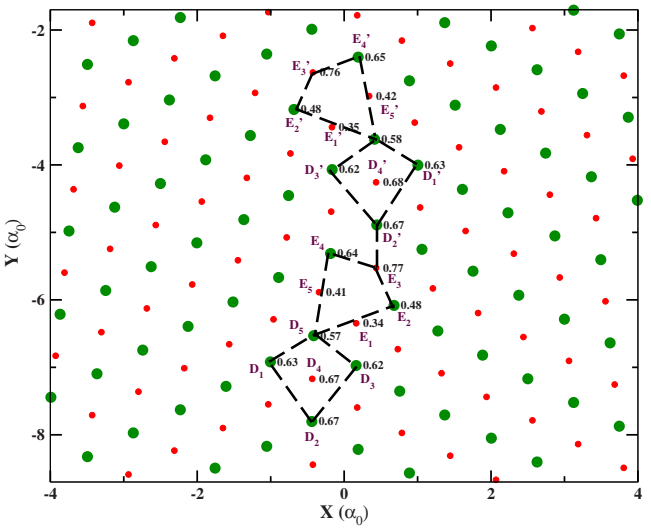

FIG. 10. (Color online) Free formation energy of a vacancy in the $\Sigma33(554)[1\bar{1}0]$ GB core structure. The big circles denote the (110) planes and the small ones denote the (220) planes. The numbers stand for the vacancy free formation energy in electron volts, at 700 K.

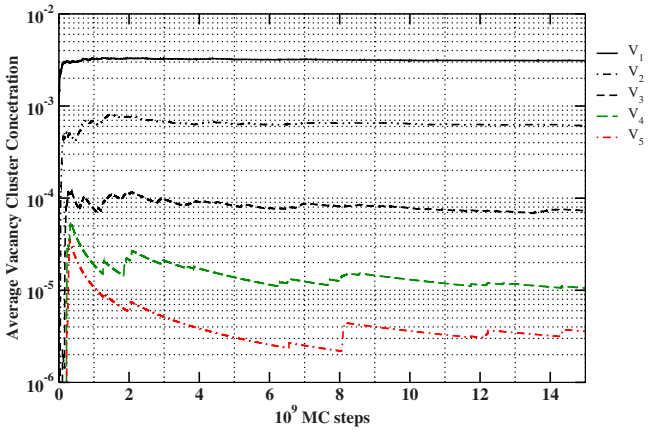

FIG. 11. (Color online) Equilibrium vacancy cluster concentration along the $[1\bar{1}0]$ lines composed of equivalent E_1 sites, in the core of $\Sigma 33(554)[1\bar{1}0]$ GB, at 700 K.

the sites D_1 and D_5 SUs (which are bulk like) show a reduction up to 0.08 eV. This is in agreement with the previous calculation in bulk Al, where the vacancy formation free energy show a small dependence with temperature.[10] The reduction is higher on site D_2: −0.14 eV. Furthermore, as the temperature is increased up to 700 K, the changes in the formation energy for the sites of E SU with respect to the values at 0 K are much higher: up to −0.17 eV. This difference could reveal a strong formation entropy contribution to the g_v^i, correlated with the strong relaxation of the local environment of the vacancies that is described in the MD section of the paper. In copper GB $\Sigma 9(221)[1\bar{1}0]$, a structure which is composed only of E units. Suzuki and Mishin[32] report higher vacancy formation entropy values on the GB sites with a lower vacancy formation energy than the bulk values.

Additionally, the formation of vacancy chains along the tilt axis, on site E_1, is observed. The other sites host only single vacancies. In the following, we consider the formation of the chains as a one-dimensional problem by considering only E_1 sites. The concentration of clusters q_l is defined by the number of clusters of length l divided by the length of the line and by averaging q_l over all equivalent $[1\bar{1}0]$ lines composed of site E_1 (two lines per CLS unit: sites E_1 and E_1'). The average concentration of vacancy clusters is given in Fig. 11. The concentration of chains of length 4 is 0.11×10^{-4} and gives us the lower limit of measurable concentration, according to our statistics, as the average concentration of the clusters composed of five vacancies did not fully convergence (it is of the order of 3×10^{-6}; Fig. 11).

TABLE I. Vacancy cluster local concentration on E_1 sites, at $T=700$ K; free formation energies and the free binding pair energy for a cluster of length l, $\epsilon_{\text{bind}}^l = \frac{l \times g_1 - g_l}{l-1}$.

Cluster size l	Local concentration	Free formation energy (eV)	Free binding energy (eV)
1	$0.311 \pm 0.003 \times 10^{-2}$	0.348 ± 0.001	
2	$0.61 \pm 0.03 \times 10^{-3}$	0.446 ± 0.003	0.250 ± 0.003
3	$0.73 \pm 0.08 \times 10^{-4}$	0.574 ± 0.007	0.235 ± 0.003
4	$0.11 \pm 0.03 \times 10^{-4}$	0.69 ± 0.02	0.234 ± 0.005

Following Yilmaz and Zimmermann,[34] we derive analytical formulas for the cluster distribution obtained by a one-dimensional Ising model in the grand canonical ensemble (Appendix). The concentration of vacancy clusters on E_1 sites is small enough (Fig. 11) to consider a dilute limit approximation which gives:

$$\frac{q_l}{n} = e^{-g_v^l / K_B T}, \tag{7}$$

where n is the total number of E_1 sites, q_l is the number of cluster of length l, and g_v^l is the free formation energy of a cluster of length l.

Table I gives the free energies obtained from the MC concentrations by inverting Eq. (7), together with the free binding pair energy $\epsilon_{\text{bind}}^l = \frac{l \times g_1 - g_l}{l-1}$, which represents the effective pair interaction between vacancies along the E_1 lines. The variation in this quantity with the length of the chain is reported. We note that the value is remarkably stable and high (0.25 eV). It almost compensates the free formation energy on site E_1 (0.35 eV), which explains why large clusters are observed (up to five vacant sites). Furthermore, this strong binding contrasts with the bulk picture where DFT calculations give a repulsion[9] (−0.07 eV) for the divacancy at $T=0$ K.

In the next section, the formation free energy of clusters is calculated by another method: the Widom insertion method. We will use the comparison between the two methods to quantify the influence of the Voronoi cell border crossings, such as those analyzed in the MD simulations, and which are allowed among vacant and occupied sites in MC simulations but not in the Widom free-energy calculations.

C. Free-energy calculation by the Widom insertion method

We make the assumption that the vacancy concentration is small enough to ignore the volume change at constant pressure. In practice, t_x is not optimized during the Monte Carlo simulation or during the Widom calculation. For simplicity, the following discussion is presented in (N,p,T), with $p=0$. In a crystalline system with M sites and N particles, the vacancy formation energy in (N,p,T) is defined by the variation in the Gibbs free energy due to the formation of an extra unoccupied site. Traditionally, this is done by moving a particle on a kink on a surface step. The system has $M+1$ sites and N particles) and $g_v^1 = G_{M+1,1}(N,p,T) - G_{M,0}(N,p,T)$. The first subscript stands for the number of lattice sites and the second for the number of vacancies.[14] If we introduce a hypothetical system with $M+1$ sites and $N+1$ atoms without any vacant site, the formation energy of a single vacancy becomes

$$g_v^1 = \mu - f_1, \tag{8}$$

where $\mu = G_{M+1,0}(N+1,p,T) - G_{M,0}(N,p,T)$ is the chemical potential of the system and $f_1 = G_{M+1,0}(N+1,p,T) - G_{M+1,1}(N,p,T)$. The term f_1 is the free-energy difference

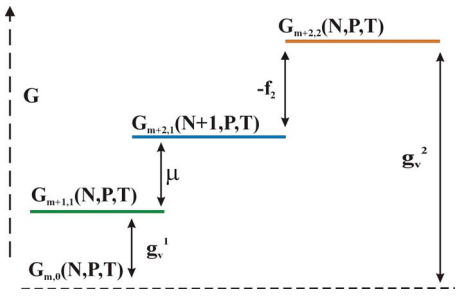

FIG. 12. (Color online) Schematic diagram of formation free-energy calculation of a divacancy, the term f_2 can be calculated by Widom particle insertion method.

between systems which have the same number of sites but a difference of one in the number of particles. It can be calculated by the Widom particle insertion method.[13]

Additionally, we can define the formation energy of a dimer (g_v^2) as the variation in the Gibbs free energy of a crystal with M sites by the formation of two vacancies on specific GB sites in nearest neighbor position. We can consider two vacant sites E_1 aligned along the tilt axis of the GB:

$$g_v^2 = G_{M+2,2}(N,p,T) - G_{M,0}(N,p,T). \tag{9}$$

We can introduce again two hypothetical systems with $G_{M+1,1}(N,p,T)$ and $G_{M+2,1}(N+1,p,T)$ and the Eq. (9) becomes

$$g_v^2 = G_{M+2,2}(N,p,T) - G_{M,0}(N,p,T) + G_{M+1,1}(N,p,T) - G_{M+1,1}(N,p,T) + G_{M+2,1}(N+1,p,T) - G_{M+2,1}(N+1,p,T). \tag{10}$$

With the proper matching of terms, we have $g_v^1 = G_{M+1,1}(N,p,T) - G_{M,0}(N,p,T)$, $\mu = G_{M+2,1}(N+1,p,T) - G_{M+1,1}(N,p,T)$, and $f_2 = G_{M+2,1}(N+1,p,T) - G_{M+2,2}(N,p,T)$. Equation (10) becomes

$$g_v^2 = g_v^1 + \mu - f_2. \tag{11}$$

Figure 12 shows a schematic representation of the free-energy levels which are used to calculate the formation energy of a divacancy.

The formation free energy of a vacancy cluster of length l is given by the following generalized equation:

$$g_v^l = g_v^{l-1} + \mu - f_l, \tag{12}$$

where ($l \geq 2$), g_v^{l-1} is the vacancy formation energy of a cluster of length $l-1$ (V_{l-1}), and f_l is the free-energy difference $f_l = G_{M+l,l-1}(N+1,p,T) - G_{M+l,l}(N,p,T)$ of a system with $M+l$ sites, $l-1$ vacant sites, and $N+1$ atoms with a system of same number of sites, l vacant sites, and N atoms.

1. Results and Discussions

The procedure described above is used to calculate the free formation energy of clusters aligned along the $[1\bar{1}0]$ lines on E_1 sites, at $T=700$ K. We perform Monte Carlo simulations in the constant lattice site ensemble at constant volume, without Voronoi border crossings. First, the structure of the GB with a vacancy cluster V_l is equilibrated by performing 1.5×10^9 MC steps with displacement moves only. Next, another 1.5×10^9 MC displacement steps are necessary, proposed only in a zone of $2a_0$ radius around the chain, in the mean time, insertions are performed in order to calculate f_l term by the Widom particle insertion method. Moreover, five replicas are used, to get a better accuracy.

TABLE II. Vacancy cluster free energy on the column of equivalent site E_1 by Widom method.

Cluster size l	Free formation energy (eV)[a]	Free pair binding energy (eV)[b]	Pair binding energy (eV)[c]
1	0.353 ± 0.004		
2	0.380 ± 0.007	0.33 ± 0.01	0.38
3	0.51 ± 0.02	0.27 ± 0.01	0.37
4	0.60 ± 0.03	0.27 ± 0.01	0.38
5	0.66 ± 0.03	0.28 ± 0.01	0.38

[a] $T=700$ K.
[b] $T=700$ K.
[c] $T=0$ K.

In Table II, we give the formation free energy of the vacancy clusters with a length ranging from one to five. In all these cases, the reference state for the formation energy of V_l cluster is the formation energy of the V_{l-1} cluster. The length of the cluster is increased one by one by adding a new vacancy at its edge. These results are in good agreement with the grand canonical MC scheme. The vacancy free formation energy for the single vacancy on the site E_1 is 0.353 eV by the Widom particle method and 0.348 eV by MC. The Widom method slightly overestimates the formation free energy of the single vacancy as the flip-flop moves of the neighbor sites of the vacant sites are prohibited. The vacancy is forced to be localized on same site. This also gives a systematic difference in free formation energy of the chains, of the order of 0.025 eV per atom, which is quite large: 10% of the pair energy. This difference propagates in the calculation of the binding energies and the differences between the formation energies appear larger. This shows the importance of allowing border crossings in Monte Carlo between vacant and occupied sites.

2. Vacancy pair binding energy

In Table III, we present the formation free energy of a pair of vacancies along the tilt axis on site E_1 as a function of the distance between the two vacancies. The binding energy of the vacancy dimer has the value 0.33 eV. This drops to 0.03eV for the pair in second-neighbor configuration and further drops to 0.01 eV in third neighbor position. The relaxation of a dimer's local environment is strong when the vacant sites lay in first neighbor position. This relaxation is restored when the vacant sites are separated and lay in second or third neighbor positions. These are in agreement with calculations at 0 K where the divacancy binding drops to zero for a distance equal or greater than the third neighbors along the tilt axis. Therefore, we can consider only first

TABLE III. Formation and binding energy of a divacancy cluster along the tilt axis at site E_1 by Widom method as a function of distance between the two vacant sites. r_0 stand for the nearest-neighbor distance $\frac{\sqrt{2}}{2}a_0$, where a_0 is the lattice constant of Bulk Al at $T=700$ K.

Distance	Free formation energy (eV)	Free pair binding energy (eV)[a]	Pair binding energy (eV)[b]
$1\times r_0$	0.380 ± 0.007	0.33 ± 0.01	0.38
$2\times r_0$	0.677 ± 0.004	0.03 ± 0.01	0.08
$3\times r_0$	0.697 ± 0.004	0.01 ± 0.01	0.01

[a] $T=700$ K.
[b] $T=0$ K.

neighbors interaction in the 1D Ising model (Appendix).

V. CONCLUSIONS

The goal of this work is to extend to grain boundaries the Monte Carlo simulation that we developed for studying superabundant vacancies in the bulk. An intermediate step is the simulation of thermal vacancies in the pure metal. This raises the issue of the definition of a vacancy in a structure where, *a priori*, nothing guarantees that extra volume is localized at specific sites. We have shown that, by intensive MD simulation, the symmetrical tilt boundary $\Sigma=33(554)[1\bar{1}0]$ is stable enough, at $T\leq 700$ K, to map the atomic positions on the lattice defined by the geometrical CSL model. The vacancies diffuse, sometimes by complex mechanisms involving many atoms and which require that the vacancy be dissolved. These are rare events and the vacancies are most of the time localized, even when they cluster. From these observations, we concluded that the characterization of the microstates by a combination of site occupancies, defined on the CSL lattice of the grain boundary, and continuous displacement variables is a good enough approximation. Based on this description, Monte Carlo simulations are performed in the Grand Canonical ensemble, with the constraint that the GB core structure is fixed by the choice of the lattice. Space is continuously decomposed in cells by the Voronoi procedure. The Monte Carlo simulations are composed of insertion/deletion moves in the cells (spin flips) and displacement moves confined in the cells. Even if the calculation is computationally demanding, owing to the large dimension of phase space, intergranular vacancy concentrations are obtained from the average occupancies. The grace of the use of a lattice is that a lattice-gas model can be defined. The parameters, free formation energy of the isolated vacancy and free binding pair energies, are computed by the Widom insertion method and from the MC concentrations by an inverse method. The comparison between the two shows that forbidding the cell crossings between a vacancy and its neighbors can result in an error of the order of 10% on the free binding pair energies which accumulate in the computation of the free formation energies of vacancy clusters, therefore leading to large errors. Free formation energies of isolated vacancies are in very good agreement with the concentrations obtained by MC.

The stability of the vacancies in this GB makes it a good candidate to continue the extension of the method by introducing solute interstitials (hydrogen) and lowering the temperature, with the final goal to simulate, in a realistic way, superabundant vacancies at a grain boundary. The issue of the definition of the grid size is important, especially at high temperature, if the solid becomes highly defected (not the case of the GB studied in the paper). We propose that MD be used, on a time scale which gives a reasonable estimate of the self-diffusion coefficient, to monitor double occupancies of the grid cells. Then this grid can be refined until no double occupancy is detected, which guarantees that most relevant microstates are considered in the MC simulation. The notion of lattice site is lost in this case.

ACKNOWLEDGMENTS

It is a pleasure to thank Michel Mareschal for his support, and Bernard Legrand and Florin Nita for their comments on the manuscript. One of us (E.V.) warmly thanks T.E. Karakasidis for fruitful discussions. We acknowledge the Rhône Alpes Region (Grant No. 05-029428-01, bourse d'accueil régionale), CECAM, and the French Agence Nationale de la Recherche (project H-inter, Grant No. ANR-06-BLAN60231) for financial support.

APPENDIX: ANALYTICAL FORMULAS FOR VACANCY CHAIN DISTRIBUTION IN THE GRAND CANONICAL ENSEMBLE

The problem of the vacancy line along the tilt axis can be treated, in an approximate way, by a one-dimensional Ising model. This means that the interaction between the vacancies on site E_1 and those on the other sites are ignored (which is not a problem at low concentrations). Furthermore, the range of interaction between vacancies on the same line is limited to the nearest neighbors. Following Yilmaz and Zimmermann,[34] the configuration dependent part of the potential energy is

$$E=-\epsilon(n_1-q)=-\epsilon\sum_{k=1}^{\infty}(k-1)q_k, \tag{A1}$$

where ϵ is the binding energy between the vacancies ($\epsilon>0$ for an attraction), n_1 is the number of vacancies, and q is the total number of clusters. We look for $\{\overline{q_k}\}$, the average distribution of clusters. q_k is the number of clusters of length k in a line composed of n sites. The partition function in the grand canonical ensemble is

$$Q=\sum_{n_1=1}^{n}e^{-\mu n_1/kT}\sum_{q=1}^{n_1}\frac{n}{q}g_1g_2e^{-E/kT}, \tag{A2}$$

where μ is the Lagrange multiplier used to express that the total number of vacancies n_1 fluctuates but that its average is fixed (the meaning of μ is cleared below). g_1 and g_2 can be expressed as a function of factorials of n_1, $n-n_1$, and n (Ref. 34). g_1 represents the number of ways to separate n_1 vacancies in q clusters, and g_2 is the number of ways to separate $(n-n_1)$ particles in q clusters. The product gives the number

of microstates, in this 1D model, which have the energy $E=-\epsilon(n_1-q)$ (degeneracy). The maximum term method is first applied to the inner sum in Eq. (A2), optimizing $t=\frac{n}{q}g_1g_2e^{-E/kT}$ with respect to q, at fixed n_1, such as in the canonical ensemble. This gives

$$\frac{q^*(n_1)}{n}=\frac{\sqrt{1+4(e^{\epsilon/kT}-1)\frac{n_1}{n}\frac{n-n_1}{n}}-1}{2(e^{\epsilon/kT}-1)}, \tag{A3}$$

and the partition function is approximated by

$$Q\approx\sum_{n_1=1}^{n}e^{-\mu n_1/kT}t^*(n_1),$$

where t^* is the maximum term which corresponds to q^*. The maximal term method applied a second time, with respect to n_1, gives

$$\frac{n_1-1}{n-n_1}\frac{n-n_1-q^*}{n_1-q^*}=e^{(\mu-\epsilon)/kT}. \tag{A4}$$

Eqs. (A3) and (A4) are coupled equations of n_1 and q^* that have to be solved numerically for each value of $e^{(\mu-\epsilon)/kT}$. Then the cluster distribution $\{q_i\}$ is obtained by the same method as in the Canonical ensemble[34] with n_1^* and q^* fixed:

$$q_i=S_1^iS_2, \tag{A5}$$

$$S_1=1-\frac{q^*}{n_1^*}, \tag{A6}$$

$$S_2=\frac{q^{*2}}{n_1^*-q^*}. \tag{A7}$$

In the dilute limit, $\frac{n_1}{n}=\theta_1\ll 1$, Eq. (A3) is expanded to second order in θ_1 and combined to Eq. (A4) to get θ_1. Finally, Eqs. (A5)–(A7), developed to first order, give

$$\frac{q_i}{n}=e^{-[i\mu-(i-1)\epsilon]/kT},$$

where $i\mu-(i-1)\epsilon$ is the free formation energy of a cluster of length i if we consider that μ is the free formation energy of an isolated vacancy and ϵ is the effective free binding energy between two vacancies in first neighbor position. The evaluation of those quantities by the Widom insertion method and the comparison with the results obtained by Monte Carlo simulation including all degrees of freedom (distribution over all the sites of the GB and displacement of all the particles) give a satisfactory agreement which validates the hypothesis. In particular, the simple decomposition of the free energy in two terms: the formation energy of the isolated vacancy, plus an effective short-range interaction, is enough.

*Present address: Department of Computer Science, University of Ioannina, P.O. BOX 1186, 45110, Ioannina, Greece; evamvak@cs.uoi.gr
†tanguy@emse.fr

[1] Y. Kraftmakher, Phys. Rep. **299**, 79 (1998).
[2] W. Egger, G. Kogel, P. Sperr, W. Triftshauser, S. Rodling, J. Bar, and H. Gudladt, Appl. Surf. Sci. **194**, 214 (2002).
[3] T. Ishizaki, Q. Xu, T. Yoshiie, S. Nagata, and T. Troev, J. Nucl. Mater. **307-311**, 961 (2002).
[4] T. Yoshiie, T. Ishizaki, Q. Xu, Y. Satoh, and M. Kiritani, J. Nucl. Mater. **307-311**, 924 (2002).
[5] Y. Fukai, Phys. Scr. **T103**, 11 (2003).
[6] Y. Fukai, K. Mori, and H. Shinomiya, J. Alloys Compd. **348**, 105 (2003).
[7] S. M. Foiles, Phys. Rev. B **49**, 14930 (1994).
[8] R. Najafabadi and D. J. Srolovitz, Phys. Rev. B **52**, 9229 (1995).
[9] K. Carling, G. Wahnstrom, T. R. Mattsson, A. E. Mattsson, N. Sandberg, and G. Grimvall, Phys. Rev. Lett. **85**, 3862 (2000).
[10] K. M. Carling, G. Wahnstrom, T. R. Mattsson, N. Sandberg, and G. Grimvall, Phys. Rev. B **67**, 054101 (2003).
[11] V. Rosato, M. Guillope, and B. Legrand, Philos. Mag. A **59**, 321 (1989).
[12] B. Loisel, J. Lapujoulade, and V. Pontikis, Surf. Sci. **256**, 242 (1991).
[13] D. Tanguy and M. Mareschal, Phys. Rev. B **72**, 174116 (2005).
[14] S. Pronk and D. Frenkel, J. Phys. Chem. B **105**, 6722 (2001).
[15] P. R. Schwoebel, S. M. Foiles, C. L. Bisson, and G. L. Kellogg, Phys. Rev. B **40**, 10639 (1989).
[16] W. Swope and H. Andersen, J. Chem. Phys. **102**, 2851 (1995).
[17] K. Bagchi, H. C. Andersen, and W. Swope, Phys. Rev. Lett. **76**, 255 (1996).
[18] M. Guillopé, J. Phys. (France) **47**, 1347 (1986).
[19] J. D. Rittner and D. N. Seidman, Phys. Rev. B **54**, 6999 (1996).
[20] H. Van Swygenhoven, P. M. Derlet, and A. Hasnaoui, Phys. Rev. B **66**, 024101 (2002).
[21] W. C. Swope and H. C. Andersen, Phys. Rev. A **46**, 4539 (1992).
[22] F. Cleri and V. Rosato, Phys. Rev. B **48**, 22 (1993).
[23] G. Ciccotti, M. Guillope, and V. Pontikis, Phys. Rev. B **27**, 5576 (1983).
[24] A. Suzuki and Y. Mishin, Interface Sci. **11**, 425 (2003).
[25] F. Ercolessi and J. Adams, Europhys. Lett. **26**, 583 (1994).
[26] A. M. Raphuthi, X. Q. Wang, F. Ercolessi, and J. B. Adams, Phys. Rev. B **52**, R5554 (1995).
[27] K. Moriguchi and M. Igarashi, Phys. Rev. B **74**, 024111 (2006).
[28] D. Tanguy and T. Magnin, Philos. Mag. **83**, 3995 (2003).
[29] F. Sansoz and J. Molinari, Acta Mater. **53**, 1931 (2005).
[30] W. Humphrey, A. Dalke, and K. Schulten, J. Mol. Graph. **14**, 33 (1996).
[31] D. Rapaport, *The Art of Molecular Dynamics Simulation* (Cambridge University Press, Cambridge, 1995).
[32] A. Suzuki and Y. Mishin, Interface Sci. **11**, 131 (2003).
[33] F. James, Comput. Phys. Commun. **79**, 111 (1994).
[34] M. B. Yilmaz and F. M. Zimmermann, Phys. Rev. E **71**, 026127 (2005).